Science and Technology Indonesia
e-ISSN:2580-4391 *p*-ISSN:2580-4405
Vol. 11, No. 3, July 2026

Research Paper

Molecular Interaction and Crystalline Structure Reorganization of *C. esculenta* and *M. leucadendra* Extract-Loaded CS/PVA Electrospun Nanofibers

Atina[1,5], Idha Royani[2,3], Assa Idah[3], Miksusanti[4], Fitri Suryani Arsyad[2,3*]

[1]*Doctoral Program, Faculty of Mathematics and Natural Science, Universitas Sriwijaya, Ogan Ilir, South Sumatra, 30862, Indonesia*
[2]*Department of Material Science, Postgraduate Program, Universitas Sriwijaya, Palembang, 30139, Indonesia*
[3]*Department of Physics, Faculty of Mathematics and Natural Science, Universitas Sriwijaya, Ogan Ilir, South Sumatra, 30862, Indonesia*
[4]*Department of Pharmacy, Faculty of Mathematics and Natural Science, Universitas Sriwijaya, Ogan Ilir, South Sumatra, 30862, Indonesia*
[5]*Department of Physics, Faculty of Science and Technology, Universitas PGRI Palembang, Palembang, 30123, Indonesia*
*__Corresponding author__: fitri_suryani@unsri.ac.id

Abstract
Understanding the molecular-to-structural evolution of extract-loaded electrospun systems is essential for rationally designing biofunctional nanomaterials. In this study, chitosan/polyvinyl alcohol (CS/PVA) electrospun nanofibers incorporated with *Colocasia esculenta* (CE) and *Melaleuca leucadendra* (ML) extracts were systematically investigated to elucidate the correlation between precursor solution interactions and resulting fiber morphology. Raman and UV-Visible spectroscopy were employed to probe molecular interactions and electronic transitions in electrospinning solutions. Extract incorporation induced vibrational band broadening and intensity suppression in Raman spectra, accompanied by increased absorbance and a red shift in UV–Visible spectra, particularly in the ML-containing system, indicating enhanced hydrogen bonding and greater electronic delocalization. Following electrospinning, structural characterization using XRD, FTIR, and SEM revealed progressive crystallinity reduction, peak shifting toward lower diffraction angles, hydrogen-bond-driven band broadening, and morphological evolution from smooth 90.86 ± 1.87 nm fibers (CS/PVA) to thicker 111.89 ± 2.96 nm fibers (CS/PVA/CE) and 118.48 ± 2.98 nm fibers (CS/PVA/ML). No separate crystalline extract phase was detected, confirming molecular-level dispersion within the polymer matrix. The ML-modified system exhibited the highest degree of amorphization and structural reorganization. These results establish a direct structure–property–function relationship, demonstrating that extract-induced modulation of intermolecular interactions governs crystalline organization, electrospinning dynamics, and nanofiber morphology. This study provides mechanistic insight into crystallinity engineering in plant-extract-loaded polymer systems and offers a scalable strategy for designing advanced bioactive electrospun nanomaterials.

Keywords
Electrospun Nanofibers, Chitosan/PVA, *Colocasia esculenta*, *Melaleuca leucadendra*, Molecular Interactions

Received: 24 January 2026, Accepted: 27 March 2026
https://doi.org/10.26554/sti.2026.11.3.795-807

1. INTRODUCTION

Nanofibers produced through an electrospinning process based on a mixture of natural and synthetic polymers have attracted increasing attention due to their unique structural features, high surface-to-volume ratio, and tunable physicochemical properties, which are highly desirable for advanced functional materials (Xing et al., 2023). Among various polymer systems, chitin (CS) has been extensively explored due to its biocompatibility, biodegradability, and natural biological activity (Azmana et al., 2021). However, the rigid molecular structure and limited solubility of chitosan often limit its solubility, especially in electrospinning applications (Jin et al., 2022). To overcome these limitations, polyvinyl alcohol (PVA) is often mixed with chitosan to improve chain bonding, solution stability, and fiber formation capabilities, resulting in uniform and continuous nanofiber mats (Cui et al., 2021).

In recent years, the integration of natural plant extracts into polymer nanofibers has emerged as a promising strategy for imparting additional bio-functional properties, such as antioxidant activity (Fahimirad et al., 2021) and antimicrobial activity (Maleki et al., 2024), while maintaining environmental sustainability. Plant extracts generally contain a complex mixture of secondary metabolites (Carvalho et al., 2021), including phenolics, flavonoids, and terpenoids, which can interact with the polymer matrix through hydrogen bonds and other intermolecular forces. Despite its potential, the integration of plant extracts into electrospun fibers remains challenging due to the possibility of phase separation, changes in solution chemistry,

and changes in fiber morphology.

Previous studies have largely focused on evaluating the biological performance of extract-loaded nanofibers (Idjan et al., 2025; Naeimi et al., 2020), with little attention given to the fundamental physicochemical transformations that occur during the transition from polymer solution to electrospun fiber. Specifically, the role of plant extracts in modifying molecular interactions in the CS/PVA solution and how these interactions govern the structural and morphological characteristics of the resulting nanofibers is not yet fully understood. Furthermore, most reports rely on post-electrospinning characterization techniques, such as FTIR or SEM (Sun et al., 2022; Anaya-Mancipe et al., 2023), without systematically correlating the spectroscopic signatures of the precursor solution with the structural features of the final fiber material.

Spectroscopy techniques, including Raman and UV-Visible spectroscopy, provide powerful tools for analyzing molecular interactions and electronic transitions in polymer solutions prior to the electrospinning process. Raman spectroscopy is highly sensitive to changes in molecular vibrations (real time) and chemical environments (Zou et al., 2025; Xiao et al., 2025), while UV-Visible spectroscopy provides insight into optical absorption behavior associated with conjugated compounds or chromophores present in plant extracts. When combined with structural and morphological analysis of electrospun fibers using X-ray diffraction (XRD), Fourier transform infrared spectroscopy (FTIR), and scanning electron microscopy (SEM), a comprehensive understanding of the structure-property relationship can be achieved.

Despite the growing number of studies on plant-extract-loaded electrospun nanofibers, most investigations primarily focus on the biological functionality or post-electrospinning characterization of the resulting fibers. However, the fundamental physicochemical processes that occur during the transition from polymer solution to electrospun nanofiber remain insufficiently understood. In particular, how plant extracts modify molecular interactions within the precursor CS/PVA solution and how these changes subsequently influence the structural organization and morphology of the electrospun fibers has rarely been systematically explored. The novelty of this work lies in the combined spectroscopic investigation of precursor electrospinning solutions using Raman and UV–Visible spectroscopy together with comprehensive post-electrospinning structural characterization using XRD, FTIR, and SEM. This integrated approach enables a direct correlation between solution-phase molecular interactions and the resulting nanofiber structural properties, providing new insight into the physicochemical mechanisms governing the formation of plant-extract-modified CS/PVA nanofibers.

Therefore, in this study, we present a systematic investigation of CS/PVA-based electrospun nanofibers enriched with two different plant extracts, namely *Colocasia esculenta* (CE) and *Melaleuca leucadendra* (ML). Three polymer solutions (CS/PVA, CS/PVA/CE, and CS/PVA/ML) were analyzed using Raman and UV–Visible spectroscopy to understand the effect of extract addition on molecular interactions and optical properties. Furthermore, these solutions were electrospun under controlled conditions to produce nanofibers, which were then analyzed using XRD, FTIR, and SEM to evaluate their structural organization, chemical bonds, and morphological characteristics. By establishing a direct correlation between the spectroscopic features in the solution phase and the fiber structure in the solid phase, this study provides new insights into the physicochemical mechanisms governing the formation of extract-loaded CS/PVA nanofibers, providing a rational basis for the design of multifunctional bio-based nanomaterials.

2. EXPERIMENTAL SECTION

2.1 Materials

Chitosan (CS) with a medium molecular weight and a degree of deacetylation of approximately 75% is used as a natural polymer matrix. Polyvinyl alcohol (PVA) from EMSURE® (Merck Group) with an average molecular weight of 60 kDa and a degree of hydrolysis of 98% is used to improve the solubility of the polymer solution. Plant extracts, labeled CE and ML, were obtained from an extraction process using the maceration method as described in study (Baro et al., 2023) to obtain a crude extract. Acetic acid solution (60% v/v) and deionized water were used as solvents without further filtration. All chemicals were of analytical grade and were used in their original form.

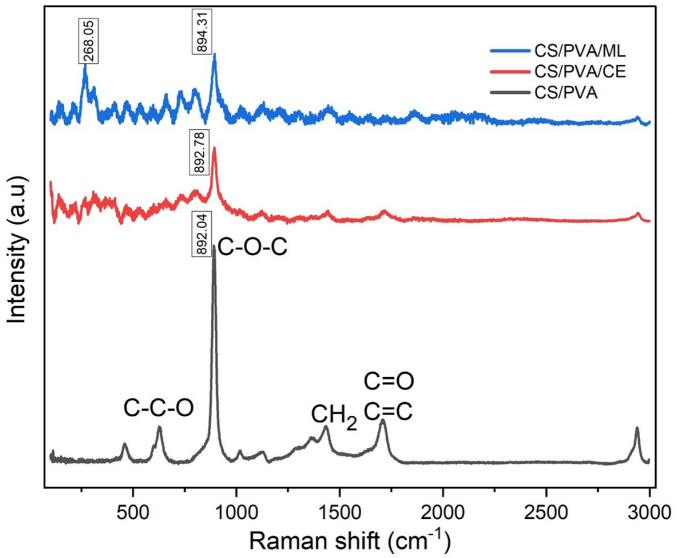

Figure 1. Raman Spectrum of the Electrospinning Solution

2.2 Methods

2.2.1 Extraction

Plant extracts were prepared using the maceration method in accordance with the procedures described by Dzigbor et al. (2025), Miksusanti et al. (2025), and Aruan et al. (2017). Briefly, dried and ground leaves of *Colocasia esculenta* and *Melaleuca leucadendra* were mixed with ethanol (96%) at a solid-to-solvent

ratio of 1:10 (w/v). The mixture was stirred and left to stand in a dark room at room temperature for 5 × 24 hours to ensure adequate extraction of bioactive compounds. The extract was then filtered using Whatman filter paper to remove solid residues. The filtrate was concentrated using a rotary evaporator at 50 °C to remove the solvent and obtain a concentrated extract. The concentrated extract was stored at 4 °C prior to use.

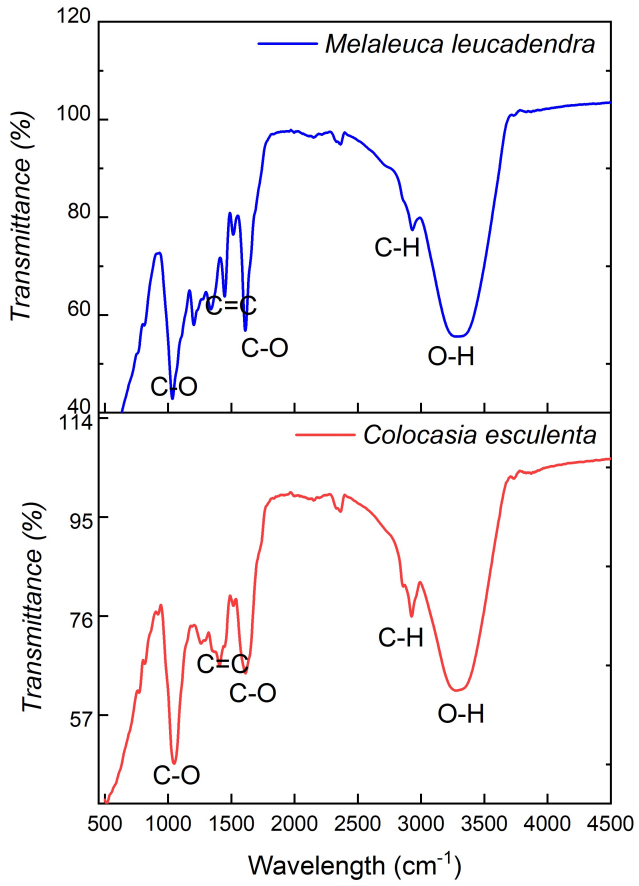

Figure 2. FTIR Spectra of *C. esculenta* and *M. leucadendra* Extracts

2.2.2 Preparation of Polymer Solutions

Three types of polymer solutions were prepared for the electrospinning process, namely CS/PVA, CS/PVA/CE, and CS/PVA/ML. CS was dissolved in 60% acetic acid, stirred with a magnetic stirrer for 4 hours at a temperature of 45 °C to obtain a CS solution of 0.03 g/mL (Duan et al., 2023). PVA and distilled water were mixed at a ratio of 7:3 and stirred for 2 hours at 45 °C (Jin et al., 2022). The CS and PVA solutions were mixed at a ratio of 3:7 and stirred for 1 hour to obtain a homogeneous CS/PVA solution. For solutions containing extracts, CE or ML extracts were added to the CS/PVA solution at a concentration of 3% by weight relative to the total polymer content. The resulting solution was stirred further for 2 hours to achieve extract homogeneity. All solutions were stored at room temperature for use as electrospinning solutions.

2.2.3 Raman Spectroscopy of Polymer Solutions

Raman spectroscopy was performed to investigate molecular interactions and functional groups present in the polymer solution prior to the electrospinning process. Raman spectra were obtained using a Horiba Micro Confocal Raman Fast Imaging spectrometer, with a focal length of 800 mm, a 785 nm laser source, wavenumber range of 100-3000 cm^{-1} and an open electrode thermoelectrically-cooled detector to -60 °C, a 600 gr/mm grating, and a 10× objective lens. Raman spectroscopy was equipped with LabSpec 6 software with NavSharp, ViewSharp, and MVAPlus to capture the spectrum.

2.2.4 UV-Visible Spectroscopy

The UV-Visible absorption spectrum of the polymer solution was recorded to determine the optical absorption characteristics and identify the presence of chromophores associated with the extract. The maximum absorption wavelength of each solution was measured using a Thermo Scientific Genesys 150 spectrophotometer in the wavelength range of 200-800 nm at room temperature and distilled water as a blank.

2.2.5 Electrospinning Process

Electrospinning was performed using a Nachriebe Electrospinning series 601 with a standard horizontal electrospinning setup. The viscosity of the solution was measured using an Ostwald viscometer with distilled water as the standard solution. Each polymer solution was placed in a plastic syringe equipped with an 18G 10 mL stainless steel needle. The electrospinning process was carried out using a high-voltage power supply under ambient conditions. During electrospinning, a voltage of 16 kV was applied between the needle and the grounded collector (Juncos Bombin et al., 2020). The solution flow rate was controlled using a syringe pump set at 0.4 mL h^{-1} (Yang et al., 2024), while the distance between the needle tip and the collector was maintained at 12 cm (Angel et al., 2020). Electrospinning was performed under environmental conditions of 25 °C and relative humidity below 50% (Qin et al., 2022). Under these conditions, a stable Taylor cone and continuous nanofiber jet were obtained, resulting in uniform nanofiber deposition on the collector surface. The collected nanofibers were placed on aluminum foil attached to a static collector and then dried at room temperature for 1 × 24 hours to remove residual solvents, after which they were characterized.

2.2.6 X-ray Diffraction (XRD) Analysis

The crystalline structure of the nanofibers produced through the electrospinning process was analyzed using an X-ray diffractometer with a voltage setting of 40kV, 15 mA; equipped with a Cu Kα radiation source (λ = 1.5406 Å). Goniometer; MiniFlex 300/600, SC-70 detector. The diffraction pattern was

Table 1. XRD Analysis of CS/PVA, CS/PVA/CE, and CS/PVA/ML Nanofibers

Sample	2θ (°)	FWHM (°)	Crystallite Size (nm)
CS/PVA	19.69	2.79	2.89
CS/PVA/CE	19.36	3.89	2.07
CS/PVA/ML	19.37	7.03	1.15

Table 2. Comparison of FTIR Peaks for CS/PVA, CS/PVA/CE, and CS/PVA/ML Solutions

Wavenumber (cm^{-1})	CS/PVA	CS/PVA/CE	CS/PVA/ML	Assignment	Interpretation
~3300	✓	shifted	shifted	O–H stretching	hydrogen bonding interaction
~2920	✓	✓	↑ intensity	C–H stretching	aliphatic chains (extract contribution)
~1650	✓	shifted	shifted	C=O / amide I	interaction with extract
~1550	✓	✓	✓	N–H bending	chitosan backbone
~1080	✓	✓	✓	C–O stretching	polysaccharide structure

recorded in the 2θ range of 5.0-90.0° with a scanning speed of 10.0° min^{-1}, step width 0.0200°, incident slit 1.250°, length limiting slit 10.0 mm. The degree of crystallinity and peak positions were evaluated to assess the effect of plant extract addition on the CS/PVA matrix. The crystallite size of the electrospun nanofibers was estimated using the Scherrer equation:

$$D = \frac{K\lambda}{\beta \cos\theta}$$

where D is the crystallite size, K is the shape factor (0.9), λ is the X-ray wavelength, β is the full width at half maximum (FWHM), and θ is the Bragg diffraction angle.

2.2.7 Fourier Transform Infrared (FTIR) Spectroscopy

FTIR spectroscopy is used to identify functional groups and investigate intermolecular interactions in nanofibers produced by electrospinning. FTIR spectra were collected using the Agilent Cary 630 FTIR Spectrometer from Benchtop FTIR Instruments. Spectra were measured in the wavelength range of 680-4000 nm. All samples were analyzed in the solid state using MicroLab FTIR software.

2.2.8 Scanning Electron Microscopy (SEM)

The surface morphology and diameter of nanofibers produced through the electrospinning process were analyzed using a ZEISS EVO MA 10 SEM EDX electron microscope. Before imaging, the samples were coated with a thin layer of gold through a sputter-coating process to improve electrical conductivity. SEM images were taken at an acceleration voltage of 13 kV, with a magnification of 30,000 times. The fiber diameter distribution was determined by measuring 100 randomly selected fiber diameter points from the SEM images using ImageJ analysis software. The measurement results were analyzed using OriginPro 2025 to ensure statistical significance, and reported as the mean diameter ± standard deviation; the distribution was presented as a histogram.

3. RESULT AND DISCUSSIONS

3.1 Raman Spectroscopy of Polymer Solutions

Raman spectroscopy is used to analyze the molecular vibration characteristics and intermolecular interactions in CS/PVA-based polymer solutions prior to the electrospinning process. Figure 1 shows the Raman spectra of pure CS/PVA solutions and CS/PVA/CE and CS/PVA/ML solutions loaded with extracts in the spectral range of 100–3000 cm^{-1}.

Figure 1 shows the Raman spectrum of the electrospinning solution. The Raman spectrum of the CS/PVA solution shows several characteristic vibration modes originating from the chitosan and PVA chains. The prominent band observed around ~458 cm^{-1} is related to the vibration of the polysaccharide backbone, reflecting the collective motion of C–C and C–O bonds in the chitosan structure. The band near ~625 cm^{-1} can be attributed to C–O stretching vibrations, which are sensitive to the local hydrogen bonding environment. The well-defined peak at ~892 cm^{-1} corresponds to C–O–C stretching vibrations in glycosidic bonds, indicating the structural integrity of the chitin backbone in the mixed polymer system. The band around ~1436 cm^{-1} is attributed to CH_2 bending vibrations, mainly contributed by the PVA chain (Alibwaini et al., 2022), while the peak at ~1713 cm^{-1} is related to the C=O stretching mode (Barroso-Solares et al., 2025), possibly originating from residual acetyl groups or interchain interactions between CS and PVA (Barroso-Solares et al., 2025). Additionally, the broad band observed near ~2945 cm^{-1} corresponds to C–H stretching vibrations, which are characteristic of polymeric hydrocarbon chains. The presence and relative sharpness of these vibration modes indicate a well-blended CS/PVA system dominated by hydrogen bonding interactions, which play an important role in stabilizing the polymer solution and facilitating the electrospinning process.

The Raman spectrum of the CS/PVA/CE solution shows characteristic vibration features originating from the polymer matrix and the integrated CE plant extract. The dominant

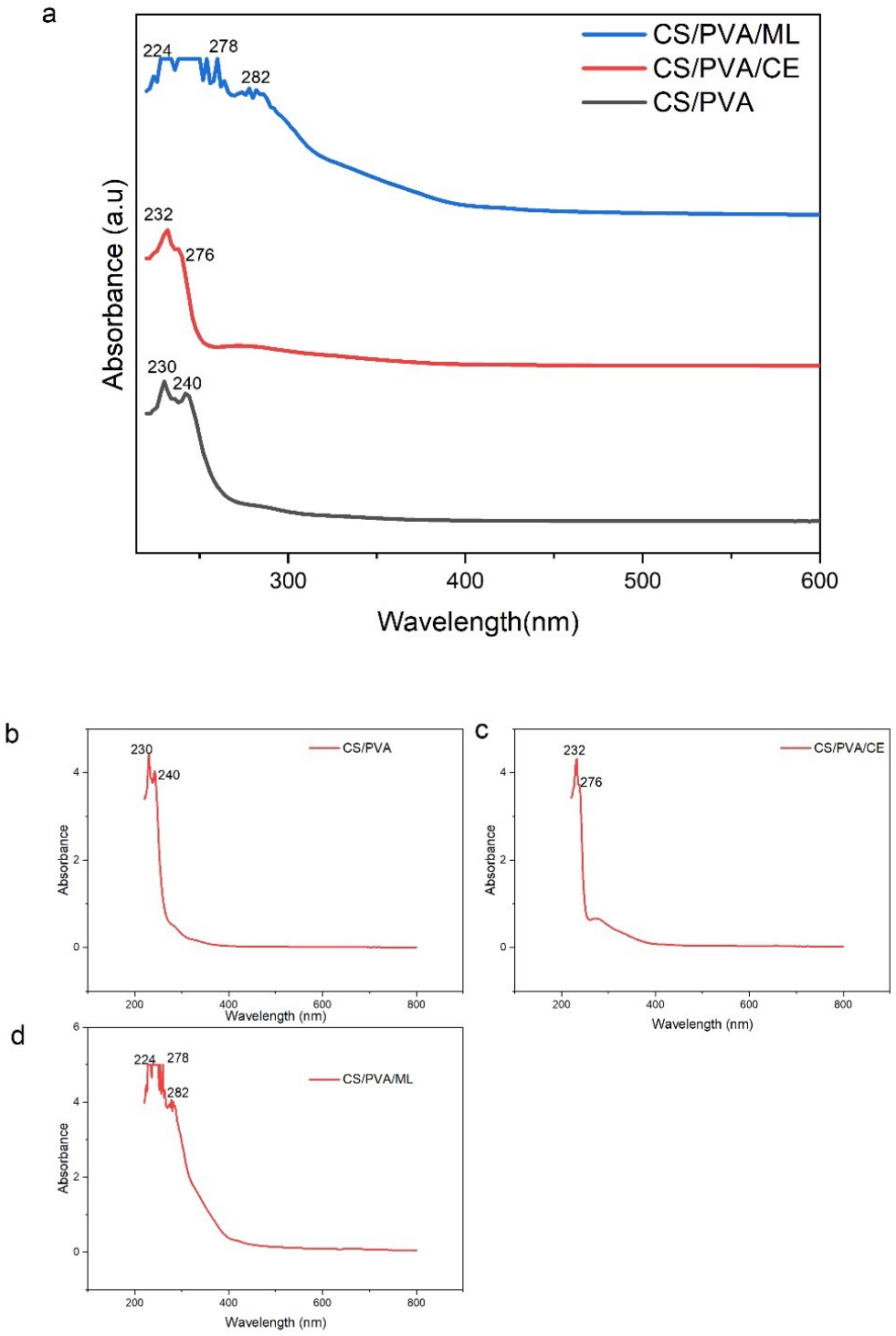

Figure 3. UV-Vis Spectrum Maximum Absorption Wavelength; a) Comparison of CS/PVA, CS/PVA/CE, and CS/PVA/ML; b) CS/PVA Solution; c) CS/PVA/CE Solution; d) CS/PVA/ML Solution

Table 3. Comparison of Electrospun CS/PVA-Based Nanofibers Reported in Previous Studies

Polymer System	Plant Extract/Additive	Fiber Diameter (nm)	Characterization Techniques	Key Findings	References
PVA	Soursop leaf and cattappa leaf extract	952–1323	FTIR, SEM, XRD, tensile test, antibacterial activity	produced nanofibers for wound healing and filtration applications	(Fitria et al., 2025)
CS/Gelat	none	103	FTIR, SEM, XRD	achieved water resistant membrane	(Alfikro et al., 2024)
CS/PVA	Eugenol	89–136	SEM, FTIR, XRD, antibacterial	enhanced antibacterial activity	(Sethuram and Thomas, 2023)

Raman band observed at around ~892 cm^{-1} is mainly associated with the C–O–C stretching vibration of the glycosidic bonds in the chitosan backbone. However, compared to the pure CS/PVA solution, this band shows a significant decrease in intensity and slight broadening. From a molecular vibration perspective, this behavior indicates a disturbance in the glycosidic environment due to the formation of intermolecular hydrogen bonds between the hydroxyl (–OH) and possibly carbonyl (C=O) functional groups of the CE extract constituents with the polymer chains (Xiao et al., 2025). Phenolic compounds commonly found in plant extracts are known to interact strongly with polysaccharides through O–H hydrogen bonds, which modify bond polarity and Raman scattering efficiency. The decrease in intensity in the mid-wave range (600–1200 cm^{-1} region) further indicates the presence of aromatic phenolic structures (Xiao et al., 2025), whose π-electron systems can cause electron delocalization effects, indirectly affecting Raman-active vibration modes in the polymer matrix. Although individual phenolic molecules cannot be identified due to spectral overlap, the Raman features are consistent with the presence of polyphenolic and flavonoid-like compounds, which are typically Raman active in this spectral region. Importantly, no sharp new crystalline Raman peaks were detected, indicating that the CE extract molecules are molecularly dispersed in the CS/PVA solution rather than forming a separate crystalline phase.

In contrast, the CS/PVA/ML solution showed more pronounced spectral modifications. Two prominent Raman bands appear at around ~268 cm^{-1} and ~894 cm^{-1}, with the latter band showing a more significant decrease in intensity and spectral broadening compared to the CS/PVA/CE system. A distinct low-frequency Raman band appears at around ~268 cm^{-1}, which is not present in the pure CS/PVA or CS/PVA/CE spectra. The appearance of a low-frequency band around ~268 cm^{-1} indicates the presence of collective lattice vibrations or modes associated with heavy atoms, which are often associated with complex aromatic or polyphenolic structures found in plant extracts (Xiao et al., 2025). The small Raman spectrum band was identified as a result of phenyl aromatic ring rotation, which is a component of phenolic compounds (Xiao et al., 2025). A more significant change in the ~894 cm^{-1} band associated with C–O–C stretching vibrations showed greater intensity suppression and spectrum broadening compared to the CE-loaded system.

A comparative analysis of three Raman spectra shows clear modulation in molecular interactions in the CS/PVA solution, depending on the extract used. Although both CE and ML extracts interact with the polymer matrix, the ML extract causes more significant disruption to the vibrational modes, as indicated by greater band broadening, decreased intensity, and the appearance of additional low-frequency modes. These findings suggest that the ML extract contains a higher proportion of rigid aromatic or polyphenolic compounds, which exert a greater influence on the vibrational dynamics of the CS/PVA system. This extract-dependent interaction mechanism provides a direct explanation for the more pronounced changes observed in fiber morphology and crystallinity in subsequent electrospun nanofibers. To support the Raman interpretation of extract-derived molecular features in the electrospinning solutions, FTIR spectra of the CE and ML extracts were analyzed.

The FTIR spectra of *Colocasia esculenta* and *Melaleuca leucadendra* extracts (Figure 2) reveal several characteristic absorption bands corresponding to functional groups commonly present in plant secondary metabolites. A broad band observed in the region of 3200–3500 cm^{-1} is attributed to O–H stretching vibrations of phenolic and alcoholic groups, indicating the presence of polyphenolic compounds capable of forming hydrogen bonds. Absorption bands around 2850–2950 cm^{-1} correspond to aliphatic C–H stretching vibrations, suggesting the presence of hydrocarbon chains associated with terpenoid components, particularly in *Melaleuca leucadendra*. Additional bands in the region of 1600–1700 cm^{-1} are assigned to C=O stretching or aromatic C=C vibrations, which are characteristic of flavonoids and other aromatic phytochemicals. Furthermore, peaks observed between 1000–1200 cm^{-1} correspond to C–O and C–O–C stretching vibrations associated with alcohol, ether, or glycosidic structures.

These functional groups identified in the extract FTIR spectra provide supporting evidence for the molecular features responsible for the Raman spectral changes observed in the precursor polymer solutions. In particular, the incorporation of plant extracts into the CS/PVA solution introduces aromatic and phenolic moieties that can interact with the polymer ma-

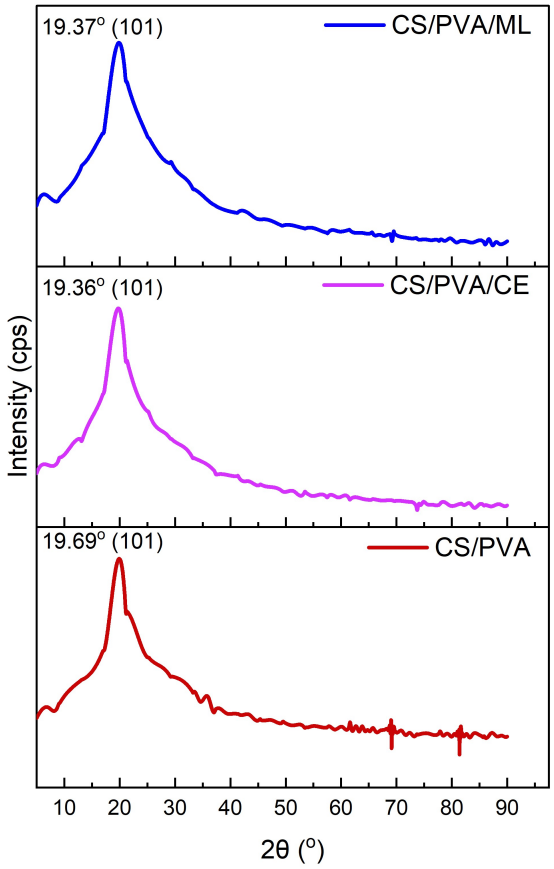

Figure 4. XRD Spectrum of CS/PVA, CS/PVA/CE, and CS/PVA/ML Nanofibers

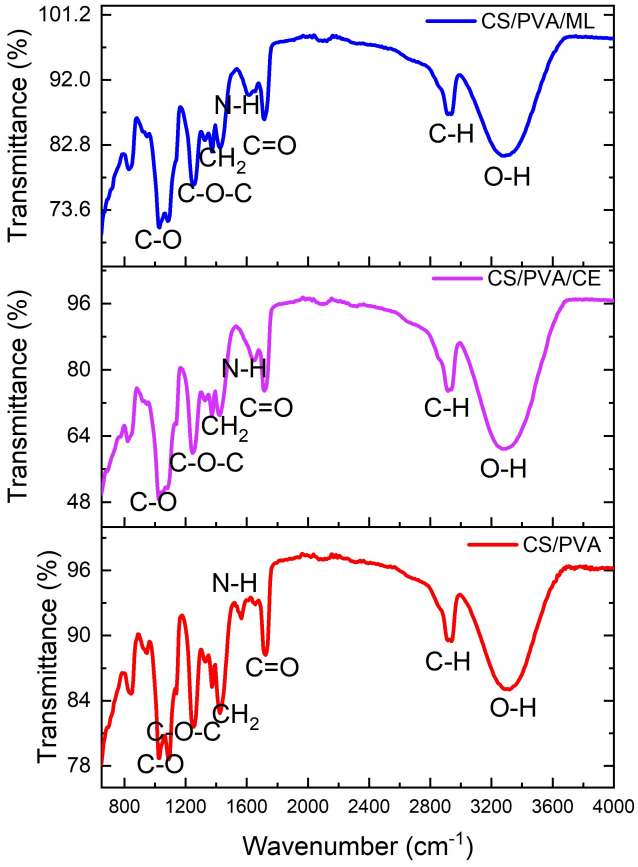

Figure 5. FTIR Spectra of CS/PVA, CS/PVA/CE, and CS/PVA/ML Nanofibers

trix through hydrogen bonding and intermolecular interactions. Such interactions modify the local chemical environment of the polymer chains, leading to observable changes in Raman vibrational bands associated with C–O, C–N, and C–H stretching modes in the CS/PVA backbone.

Compared with the pristine CS/PVA solution, the Raman spectra of CS/PVA/CE and CS/PVA/ML solutions exhibit band intensity variations and slight shifts in characteristic vibrational modes, indicating modifications in molecular interactions within the polymer network. These changes suggest that the phenolic and terpenoid compounds identified in the FTIR spectra of the extracts interact with the CS/PVA matrix, altering the hydrogen-bonding network and influencing the physicochemical structure of the precursor solution prior to electrospinning. This complementary spectroscopic approach allows a more reliable interpretation of the molecular origin of the Raman bands without relying solely on speculative compound assignments.

3.2 UV-Visible Spectroscopic Analysis of Electrospinning Solutions

UV-Visible spectroscopy was used to investigate the optical absorption characteristics and electronic transitions of CS/PVA-based electrospinning solutions, with a particular emphasis on the effect of adding plant extracts. Figure 2 shows the UV-Vis absorption spectra of CS/PVA, CS/PVA/CE, and CS/PVA/ML solutions recorded in the wavelength range of 200–800 nm.

Pure CS/PVA solutions exhibit a dominant absorption peak at around 230 nm, which is characteristic of $\pi \rightarrow \pi^*$ and $n \rightarrow \sigma^*$ electronic transitions associated with the polymer backbone. In CS/PVA solutions, absorption in this deep UV region is generally associated with non-conjugated functional groups such as hydroxyl (–OH), amino ($–NH_2$), and residual acetyl groups, which have localized electronic states. The absence of significant absorption bands in the visible region (>400 nm) indicates that the CS/PVA solution does not possess extensive conjugated or chromophore structures. This optical behavior is consistent with the Raman results, which show well-defined polymer vibrational modes with minimal electronic

interference, indicating a relatively ordered and electronically homogeneous polymer solution.

After the addition of CE extract, the CS/PVA/CE solution showed a slight shift in maximum absorption at around 232 nm, accompanied by an increase in overall absorption intensity compared to the pure CS/PVA system. This increase indicates the presence of additional electronic transitions originating from the CE extract component. From a spectroscopic perspective, this absorption feature is associated with $\pi \rightarrow \pi^*$ transitions in aromatic rings and $n \rightarrow \pi^*$ transitions in carbonyl or phenolic groups commonly found in plant-derived polyphenolic compounds. The proximity of the absorption maximum to that of CS/PVA indicates that CE extract molecules are molecularly dispersed in the polymer matrix rather than forming strongly conjugated domains. This interpretation is consistent with FTIR and Raman analysis, where the addition of CE causes a moderate decrease in intensity and broadening of the band without the emergence of new low-frequency collective modes. These results indicate that CE extract interacts primarily through local hydrogen bonds, causing limited electronic delocalization in solution.

UV-visible absorption characteristics provide important insights into the electronic structure of precursor solutions, which directly influence electrospinning dynamics. The increase in absorption intensity and shift of the absorption maximum toward the red observed in CS/PVA/ML solutions indicate higher electronic polarity and a possible increase in solution conductivity. These factors are known to affect jet stretching and instability during electrospinning, resulting in variations in fiber diameter and morphology. In contrast, the CS/PVA/CE solution showed more moderate changes in optical absorption, consistent with weaker electronic disruption and more localized molecular interactions. This explains the intermediate morphological and structural changes observed in the nanofibers produced via electrospinning. Overall, the UV–Vis results show a clear relationship between structure, properties, and process, where specific electronic features of the extract in the solution phase govern molecular interactions (Raman), electrospinning behavior, and ultimately the structure of the resulting nanofibers.

3.3 X-ray Diffraction (XRD) Analysis

Figure 4 shows the X-ray diffraction (XRD) patterns of CS/PVA, CS/PVA/CE, and CS/PVA/ML nanofibers produced by the electrospinning process, recorded in the 2θ range of 5–90°. All samples show a dominant broad diffraction peak centered at around 2θ = 19–20°, which is characteristic of semi-crystalline PVA-based systems mixed with amorphous chitin (Yan et al., 2023). The broad nature of this peak indicates that the nanofibers produced by electrospinning have an amorphous-semi-crystalline mixed structure, which is characteristic of polymer nanofibers produced by electrospinning due to rapid solvent evaporation and limited time for crystal growth.

Pure PVA generally exhibits strong diffraction peaks at $2\theta \approx$ 19.5–19.8°, which are widely indexed to the (101) crystallographic plane of monoclinic PVA crystals. Chitosan, on the other hand, exhibits characteristic reflections around $2\theta \approx 10°$ and 20°, but in mixed systems and electrospun fibers, these peaks often merge into a single broad halo due to decreased crystallinity. Therefore, the peak observed at ~19–20° in all samples is reasonably attributed to PVA-dominated crystalline domains, with chitosan contributing primarily to the amorphous background.

A small shift of the diffraction peak toward lower 2θ values was observed after the addition of CE and ML extracts (from 19.69° to ~19.36–19.37°). Based on Bragg's Law, this shift corresponds to an increase in interplanar spacing (d-spacing), indicating an expansion of the crystal lattice or an increase in structural disorder in the polymer matrix. This behavior suggests that the extract molecules are intercalated within or near the crystalline regions of PVA, disrupting chain packing and weakening intermolecular hydrogen bonds between PVA chains. No additional sharp diffraction peaks corresponding to crystalline plant extract phases were detected in the XRD patterns of CS/PVA/CE and CS/PVA/ML nanofibers. This indicates that the extracts are molecularly dispersed or amorphously embedded in the polymer matrix, rather than forming separate crystalline domains (Gómez et al., 2019). The dominant diffraction peak centered around $2\theta \approx$ 19–20° for all samples was indexed to the (101) plane of the semi-crystalline PVA domain. A slight shift of the peak toward lower diffraction angles after the addition of the extract indicates an increase in interplanar spacing and a decrease in crystalline order, caused by the disruption of polymer chain packing due to the extract.

To quantitatively evaluate the effect of plant extract incorporation on the crystalline structure, the crystallite size of the electrospun nanofibers was estimated using the Scherrer equation based on the dominant diffraction peak at $2\theta \approx$ 19–20°. As summarized in Table 1, the crystallite size decreases significantly from approximately 2.89 nm for pristine CS/PVA to 2.07 nm and 1.15 nm for CS/PVA/CE and CS/PVA/ML, respectively. This reduction in crystallite size is consistent with the observed broadening of the diffraction peaks and reflects an increase in structural disorder within the polymer matrix. The incorporation of plant extracts introduces additional intermolecular interactions, particularly hydrogen bonding between the functional groups of the extracts and the CS/PVA chains, which disrupts the regular packing of PVA crystalline domains. As a result, crystal growth is hindered during the electrospinning process, leading to smaller coherent scattering domains. Furthermore, the slight shift of the diffraction peak toward lower 2θ values, corresponding to increased interplanar spacing, supports the hypothesis of extract-induced lattice expansion and reduced crystallinity. Among all samples, CS/PVA/ML exhibits the smallest crystallite size, indicating the strongest disruption of polymer chain organization, which is consistent with the more pronounced structural disorder observed in FTIR and Raman analyses. These findings confirm that the incorporation of plant extracts plays a critical role in modulating the crystalline structure of electrospun CS/PVA nanofibers. It

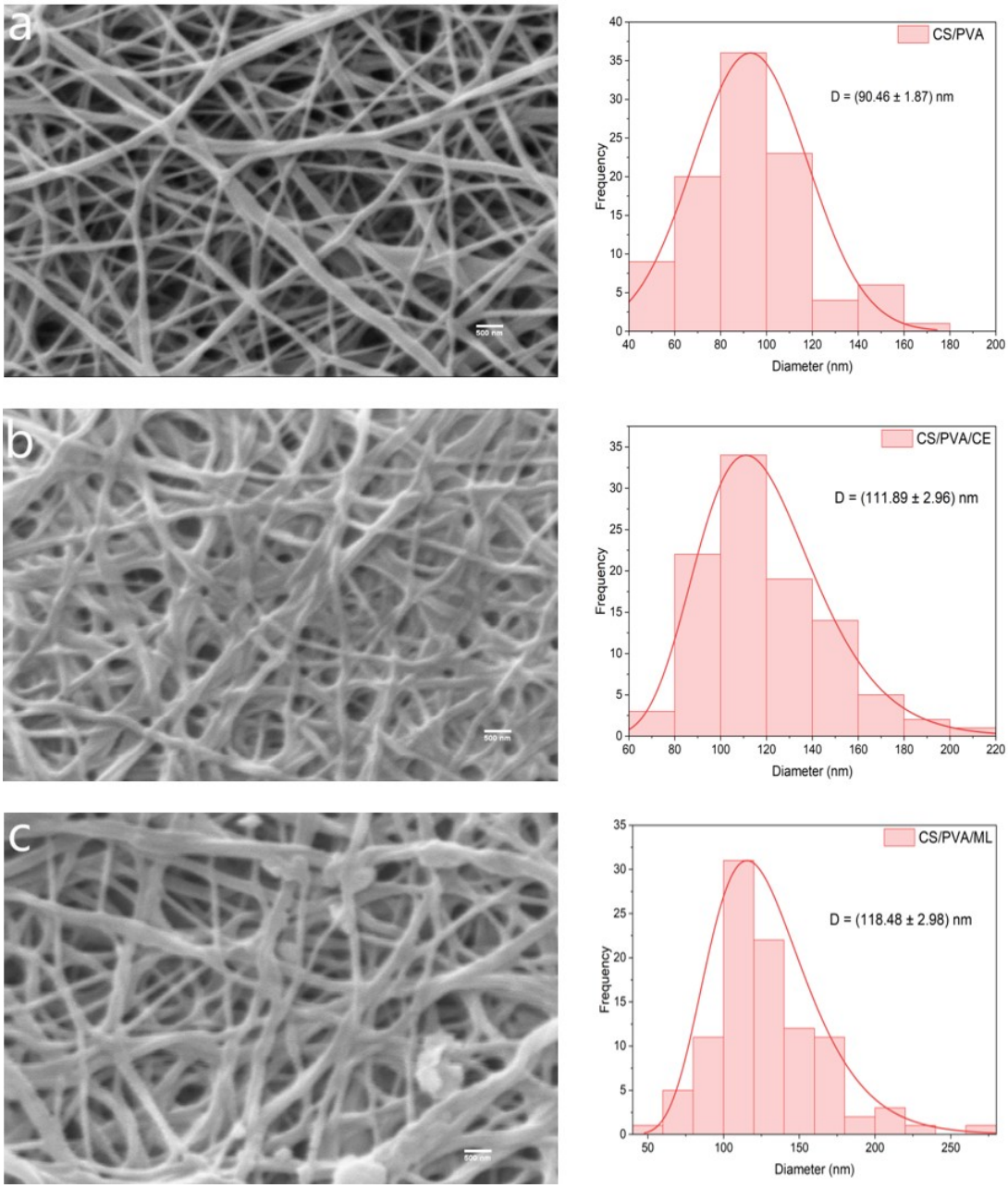

Figure 6. SEM Micrographs Electrospun and Histogram of Diameter Distribution of: a) CS/PVA Nanofibers; b) CS/PVA/CE Nanofibers; c) CS/PVA/ML Nanofibers. Scale Bar = 500 nm

should be noted that the calculated crystallite sizes represent apparent values due to the semi-crystalline nature of the polymer system and the broad diffraction peaks. Overall, these results demonstrate that plant extract incorporation serves as an effective strategy to tune the crystalline–amorphous balance in electrospun polymer nanofibers.

3.4 Fourier Transform Infrared (FTIR) Spectroscopy

FTIR analysis was performed to characterize the vibration modes of functional groups in the infrared region and to investigate possible molecular interactions within the matrix Figure 5 (CS/PVA) shows distinct and relatively sharp peaks characteristic of PVA and chitosan, with the O–H band (~3300 cm^{-1}) still relatively narrow, indicating dominant intramolecular hydrogen bonding. The crystalline domain of PVA is still intact, as indicated by a fairly intense peak at ~1140 cm^{-1} (Archana

et al., 2025). The FTIR graph of CS/PVA/CE shows that the O–H band becomes wider and shifts slightly to a lower wave number, indicating the formation of new hydrogen bonds between the polymer and the phenolic compound CE. The O–H band (~3300 cm^{-1}) is the widest and its intensity decreases in CS/PVA/ML, Amida I (~1650 cm^{-1}) shows band distortion (Yan et al., 2023), the C–O–C band (~1140 cm^{-1}) weakens significantly, and the peak in this area indicates the presence of an ester group (Zhao et al., 2022). A strong signal at 1740 cm^{-1} reflects C=O ester stretching, confirming the presence of triglycerides and esterified fatty acid components as the main constituents (Amur et al., 2025).

The strongest ML molecular interactions cause fragmentation of the PVA crystalline domain and increased amorphization of the matrix. FTIR spectra confirm the successful incorporation of CE and ML extracts into the CS/PVA electrospun nanofibers. The broadening and slight red-shift of the O–H/N–H stretching band around 3300–3400 cm^{-1} (Abdulrahman et al., 2024) indicate enhanced hydrogen bonding interactions between the polymer chains and bioactive compounds present in the extracts (Islam et al., 2024). Furthermore, the reduced intensity of the C–O–C stretching band at ~1140 cm^{-1} suggests disruption of the crystalline domains of PVA, which is consistent with the observed crystallite size reduction from XRD analysis. Among all samples, CS/PVA/ML exhibits the highest degree of structural disorder, corroborating Raman spectral broadening and UV-Visible absorption enhancement. FTIR band assignments of electrospun CS/PVA, CS/PVA/CE, and CS/PVA/ML nanofibers showing extract-induced hydrogen bonding interactions and gradual reduction of polymer crystallinity (Putri et al., 2025).

To facilitate a clearer interpretation of the FTIR spectra, a comparative band assignment table has been constructed (Table 2). The results show that the incorporation of plant extracts induces noticeable shifts in characteristic peaks, particularly in the O–H and C=O regions, indicating enhanced hydrogen bonding interactions and modification of the polymer network. These changes confirm that the extract components interact with the CS/PVA matrix at the molecular level.

3.5 Scanning Electron Microscopy (SEM)

The electrospun fibers were scanned with SEM to determine their size and distribution. The SEM scan results are shown in Figure 6. SEM analysis reveals smooth, bead-free nanofibers with interconnected porous networks for all samples. The average fiber diameter increases from 90.86 ± 1.87 nm (CS/PVA) to 111.89 ± 2.96 nm (CS/PVA/CE) and 118.48 ± 2.98 nm (CS/PVA/ML), indicating that extract incorporation significantly affects the electrospinning jet dynamics. The histogram distributions show relatively narrow diameter distributions, indicating stable jet formation during electrospinning. The increased fiber diameter can be attributed to enhanced solution viscosity (Luo et al., 2025) and intermolecular hydrogen bonding interactions, which reduce jet stretching under the applied electric field. The ML-containing fibers exhibit the largest diameter and slightly rougher surface morphology, suggesting stronger polymer–extract interactions. These findings are in strong agreement with XRD results showing reduced crystallite size, FTIR band broadening, and Raman spectral disorder, confirming that extract incorporation promotes structural amorphization within the nanofibrous matrix.

The CS/PVA nanofibers appear smooth with relatively homogeneous distribution, no significant bead formation, a randomly oriented nanofibrous network structure with high porosity, and an average diameter of 90.86 ± 1.87 nm, indicating relatively low solution viscosity. The addition of extract as an electrospinning solution increases the viscosity of the solution and affects the morphology of the electrospinning fibers (Almafie et al., 2024). CS/PVA/CE nanofibers remain continuous and without large beads with a diameter greater than CS/PVA nanofibers with a size of 111.89 ± 2.96 nm, although the network remains homogeneous but the surface is slightly rougher than CS/PVA. Increased solution viscosity causes polymer chain packing disruption, which causes the fiber diameter to increase. This condition correlates with decreased crystallinity (XRD), broadening of the O–H band (FTIR), and increased absorbance (UV-Visible). The surface of CS/PVA/ML nanofibers appears rougher with a fiber size of 118.48 ± 2.98 nm, some small agglomeration points are observed, and the diameter distribution is slightly wider. The formation of thicker fibers causes an increase in viscosity, intermolecular interactions (intense hydrogen bonding), and a decrease in crystallinity, resulting in thicker fibers. This morphology satisfied the critical parameters for wound dressing applications, namely small nanofiber diameter, absence of significant bead defects, and high structural homogeneity (Sari et al., 2025).

In electrospinning systems, solution properties such as viscosity, electrical conductivity, and surface tension collectively influence jet stability and fiber morphology. Among these parameters, viscosity plays a crucial role in determining the degree of polymer chain entanglement required for continuous fiber formation. Although conductivity and surface tension were not directly measured in this study, the incorporation of plant extracts containing polar phytochemicals may alter charge density and intermolecular interactions within the solution, potentially affecting jet elongation and fiber diameter during electrospinning. The viscosity of the electrospinning solutions was determined using an Ostwald viscometer relative to distilled water. The results show a clear increase in viscosity from 1.75 mPa.s (CS/PVA) to 2.23 mPa.s (CS/PVA/CE) and 2.52 mPa.s (CS/PVA/ML). This trend indicates enhanced intermolecular interactions and polymer chain entanglement upon incorporation of plant extracts. The higher viscosity observed in extract-loaded systems contributes to increased resistance to flow during electrospinning, which is consistent with the formation of thicker nanofibers observed in SEM analysis. These findings confirm that the addition of phytochemical compounds significantly modifies the rheological properties of the precursor solutions.

The comprehensive structural analyses reveal a strong in-

terconnection between molecular interactions, crystalline organization, morphological evolution, and optical behavior in the electrospun nanofiber system (Fitria et al., 2025). Extract incorporation enhances hydrogen bonding interactions, reduces PVA crystallinity, increases fiber diameter, and promotes structural amorphization. These changes indicate modifications in the polymer molecular environment and structural organization of the nanofibers. Such physicochemical modifications may influence the interaction of nanofibers with bioactive compounds, potentially supporting future investigations of functional properties. Among all samples, CS/PVA/ML exhibits the highest degree of structural disorder and the most pronounced structural modification, demonstrating the critical role of extract–polymer interactions in tuning the structural characteristics of electrospun nanofibers.

Although direct elemental mapping techniques such as EDS mapping or TEM were not employed in this study, the homogeneous dispersion of plant extracts within the CS/PVA matrix can be inferred from indirect evidence. The absence of phase-separated domains in SEM images, combined with relatively narrow fiber diameter distributions, suggests stable solution properties during electrospinning. Furthermore, the observed shifts and intensity changes in FTIR and Raman spectra indicate molecular-level interactions between the extract components and polymer chains, supporting the assumption of uniform dispersion within the nanofiber structure.

Due to the limited number of studies specifically reporting CS/PVA electrospun nanofibers incorporated with plant extracts, previous studies on CS-based, PVA-based, and plant-extract-loaded electrospun nanofibers are summarized in Table 3 to provide a relevant comparison with the present work.

As shown in Table 3, various electrospun nanofibers based on PVA, CS, and CS/PVA composites have been widely reported with the incorporation of plant extracts or bioactive additives to enhance functional properties such as antibacterial activity and wound healing performance. These studies typically report fiber diameters in the nanometer range and primarily rely on characterization techniques such as FTIR, SEM, and XRD to evaluate chemical structure and morphology of the resulting fibers. However, most previous investigations focus predominantly on the final fiber properties, with limited attention given to the physicochemical interactions occurring in the precursor solution prior to electrospinning. In contrast, the present study introduces a more comprehensive approach by integrating Raman and UV–Vis spectroscopy to probe molecular interactions in the precursor solution, in addition to conventional structural characterization of the electrospun nanofibers. This combined analysis enables a deeper understanding of how the incorporation of *Colocasia esculenta* and *Melaleuca leucadendra* extracts modifies intermolecular interactions within the CS/PVA matrix, which in turn influences fiber formation and morphology. Therefore, this work provides not only structural characterization but also mechanistic insight into the relationship between solution-phase interactions and nanofiber structure, which remains underexplored in previously reported systems.

4. CONCLUSIONS

This work elucidates the structure–property relationship in electrospun CS/PVA nanofibers engineered with plant-derived extracts. The incorporation of CE and ML does not generate new covalent bonds but fundamentally restructures the polymer network through intensified hydrogen bonding interactions. This molecular-level reorganization drives progressive amorphization, evidenced by FTIR and Raman band broadening, XRD crystallite size reduction, and peak attenuation of PVA crystalline domains. These structural modifications directly alter electrospinning dynamics, producing thicker nanofibers (90 → 118 nm) with modified chain packing and enhanced electronic delocalization, as supported by UV–Visible red-shift behavior. Among all formulations, CS/PVA/ML exhibits the highest structural disorder, indicating the strongest extract–polymer interaction. This study establishes controlled crystallinity modulation as an effective strategy for tuning the structural properties of bio-based nanofibers and provides a framework for the design of plant-extract-modified electrospun materials for potential biomedical applications. Future studies will focus on evaluating the biological performance of these nanofibers to further explore their potential functional applications.

5. ACKNOWLEDGEMENT

Thank you to Universitas Sriwijaya, which is author's affiliate for providing services and facilities in writing this article.

REFERENCES

Abdulrahman, M. F., A. S. Al-Rawi, L. L. Hamid, A. M. Aljumialy, W. M. Saod, and A. M. Al-Fahdawi (2024). Preparation of Polyvinyl Alcohol (PVA) Aerogel Microsphere Loaded with Biogenic Zinc Oxide Nanoparticles as Potential Antibacterial Drug. *Journal of Molecular Structure*, **1306**; 137901

Alfikro, I., Jorena, O. C. Satya, E. Koriyanti, F. Monado, and I. Royani (2024). Assessment of Different Crosslinking Mechanisms on PVA-Based Membranes to Achieve Water Resistance with Iron Imprinting Sites. *Chimica Techno Acta*, **11**(3); 6–13

Alibwaini, Y. A., O. M. Hemeda, T. Sharshar, A. H. Ashour, A. W. Ajlouni, E. A. Arrasheed, A. M. A. Henaish, and R. El-Shater (2022). Study of the PEG Content Effect on Some Properties of the PVA/PEG-EY Films Using the Raman, Positron Annihilation and Impedance Spectroscopies. *Optik*, **254**; 168591

Almafie, M. R., R. Dani, L. Marlina, J. Jauhari, and I. Sriyanti (2024). Preparation of PAN / PVDF Nanofiber Mats Loaded with Coconut Shell Activated Carbon and Silicon Dioxide for Lithium-Ion Battery Anodes. *Science and Technology Indonesia*, **9**(2); 427–447

Amur, S. A., Q. Khuhro, N. A. Soomro, Y. Oshima-Franco, A. Amur, K. H. Thebo, and A. Nadeem (2025). Biochem-

ical Characterization of Bioactive Compounds in *Citrullus colocynthis* (L.) Schrad Seed Extract Using GC–MS Analysis and Their Potential Biological Applications. *South African Journal of Botany*, **185**; 654–666

Anaya-Mancipe, J. M., V. M. Queiroz, R. F. Dos Santos, R. N. Castro, V. S. Cardoso, A. B. Vermelho, M. L. Dias, and R. M. Thiré (2023). Electrospun Nanofibers Loaded with *Plantago major* L. Extract for Potential Use in Cutaneous Wound Healing. *Pharmaceutics*, **15**(4); 1047

Angel, N., L. Guo, F. Yan, H. Wang, and L. Kong (2020). Effect of Processing Parameters on the Electrospinning of Cellulose Acetate Studied by Response Surface Methodology. *Journal of Agriculture and Food Research*, **2**; 100015

Archana, M. S., C. S. C. Lekha, S. Deepa, and N. Kalarikkal (2025). A Novel Mesoporous Taurine-Doped Polyaniline / PVA Electrospun Composite Nanofiber: Comprehensive Study. *Results in Surfaces and Interfaces*, **20**; 100610

Aruan, N. M., I. Sriyanti, D. Edikresnha, T. Sucianti, M. M. Munir, and Khairurrijal (2017). Polyvinyl Alcohol / Soursop Leaves Extract Composite Nanofibers Synthesized Using Electrospinning Technique and Their Potential as Antibacterial Wound Dressing. In *Procedia Engineering*, volume 170. pages 31–35

Azmana, M., S. Mahmood, A. R. Hilles, A. Rahman, M. A. B. Arifin, and S. Ahmed (2021). A Review on Chitosan and Chitosan-Based Bionanocomposites: Promising Material for Combatting Global Issues and Its Applications. *International Journal of Biological Macromolecules*, **185**; 832–848

Baro, M. R., M. Das, A. Kalita, B. Das, and K. Sarma (2023). Exploring the Anti-Inflammatory Potential of *Colocasia esculenta* Root Extract in In-Vitro and In-Vivo Models of Inflammation. *Journal of Ethnopharmacology*, **303**; 116021

Barroso-Solares, S., F. Lopez-Moya, T. Fraile, . A. C. Prieto, L. Lopez-Llorca, and J. Pinto (2025). Chitin and Chitosan Quantification in Fungal Cell Wall via Raman Spectroscopy. *Spectrochimica Acta Part A: Molecular and Biomolecular Spectroscopy*, **334**; 125928

Carvalho, M. T. B., H. G. Araújo-Filho, A. S. Barreto, L. J. Quintans-Júnior, J. S. S. Quintans, and R. S. S. Barreto (2021). Wound Healing Properties of Flavonoids: A Systematic Review Highlighting the Mechanisms of Action. *Phytomedicine*, **90**; 1–15

Cui, C., S. Sun, S. Wu, S. Chen, J. Ma, and F. Zhou (2021). Electrospun Chitosan Nanofibers for Wound Healing Application. *Engineered Regeneration*, **2**; 82–90

Duan, M., J. Sun, Y. Huang, H. Jiang, Y. Hu, J. Pang, and C. Wu (2023). Electrospun Gelatin / Chitosan Nanofibers Containing Curcumin for Multifunctional Food Packaging. *Food Science and Human Wellness*, **12**(2); 614–621

Dzigbor, A., D. Neglo, C. O. Tettey, and P. Alormassor (2025). Total Phenolic Content, Antioxidant Activity, GC-MS Characterization, and Antimicrobial Activity of Leaf and Flower Extracts of Porophyllum ruderale. *Pharmacological Research - Natural Products*, **7**; 100243

Fahimirad, S., H. Abtahi, P. Satei, E. Ghaznavi-Rad, M. Moslehi, and A. Ganji (2021). Wound Healing Performance of PCL/Chitosan Based Electrospun Nanofiber Electrosprayed with Curcumin Loaded Chitosan Nanoparticles. *Carbohydrate Polymers*, **259**; 117640

Fitria, S., M. R. Almafie, I. Alfikro, F. Monado, I. Sriyanti, and I. Royani (2025). Synthesis and Characterization of Polyvinyl Alcohol (PVA) Nanofiber Membranes with *Annona muricata* and *Terminalia catappa* Leaf Extract. *Science and Technology Indonesia*, **10**(3); 837–846

Gómez, D. A., J. Coello, and S. Maspoch (2019). The Influence of Particle Size on the Intensity and Reproducibility of Raman Spectra of Compacted Samples. *Vibrational Spectroscopy*, **100**; 48–56

Idjan, M. K. N. A., Fatmawati, M. R. Almafie, R. Dani, Subandrate, A. Fudholi, and I. Sriyanti (2025). Physicochemical Properties and Antioxidant Activity of PVP/CA Membranes Nanofiber Loaded *Arcangelisia flava* L. Merr. Stem Extract Using Electrospinning Technique. *Next Materials*, **8**; 100839

Islam, M., A. Javed, Z. U. Rahman, Y. O. Al-Ghamdi, and S. A. Khan (2024). Antibacterial Composite Films of Oxidized Alginate-Chitosan-ZnO Anchored Cu Nanoparticles for the Degradation of Organic Pollutants. *International Journal of Biological Macromolecules*, **278**; 134764

Jin, E., M. Wu, S. Wang, Z. Qiao, M. Li, and W. Linghu (2022). Preparation and Application Performance of Graft-Quaternization Double Modified Chitosan Electrospun Antibacterial Nanofibers. *Materials Today Communications*, **31**; 103712

Juncos Bombin, A. D., N. J. Dunne, and H. O. McCarthy (2020). Electrospinning of Natural Polymers for the Production of Nanofibres for Wound Healing Applications. *Materials Science and Engineering C*, **114**; 110994

Luo, B., H. Yang, J. Luo, K. Yu, P. Li, J. Wei, and H. Zhong (2025). Optimization of Natural Deep Eutectic Solvent Extraction Process and Activity Study of Total Flavonoids from *Dalbergia benthami* Prain. *Journal of Applied Research on Medicinal and Aromatic Plants*, **49**; 100662

Maleki, H., M. Doostan, K. Khoshnevisan, H. Baharifar, S. A. Maleki, and M. A. Fatahi (2024). *Zingiber officinale* and *Thymus vulgaris* Extracts Co-Loaded Polyvinyl Alcohol and Chitosan Electrospun Nanofibers for Tackling Infection and Wound Healing Promotion. *Heliyon*, **10**(1); e23719

Miksusanti, M., E. F. Apriani, A. Ahmadi, S. Shiyan, D. P. Wijaya, and V. A. Risanli (2025). Formulation and Characterization of Sambiloto Extract Orally Dissolving Films: A Dual Mechanism for Probiotic Growth and Antibacterial Action. *International Journal of Applied Pharmaceutics*, **17**(2); 198–203

Naeimi, A., M. Payandeh, A. R. Ghara, and F. E. Ghadi (2020). In Vivo Evaluation of the Wound Healing Properties of Bio-Nanofiber Chitosan/Polyvinyl Alcohol Incorporating Honey and *Nepeta dschuparensis*. *Carbohydrate Polymers*, **240**; 116315

Putri, A. N., A. K. Soesantyo, and E. D. Iftitah (2025). Effect of Edible Coating Material Composition Based on Chitosan-Gelatin-$CaCl_2$ and Cinnamon (*Cinnamomum verum*) Essen-

tial Oil on the Protection of Cocoa Beans (*Theobroma cacao* L.) During Storage. *Science and Technology Indonesia*, **10**(2); 528–537

Qin, Z., S. Wang, L. Wang, J. Yao, G. Zhu, B. Guo, J. Militky, M. Venkataraman, and M. Zhang (2022). Nanofibrous Membranes with Antibacterial and Thermoregulatory Functions Fabricated by Coaxial Electrospinning. *Journal of Industrial and Engineering Chemistry*, **113**; 373–379

Sari, W. F., S. Haryati, and R. Mohadi (2025). Development of Nanofiber Made of Nanocellulose with Oil Encapsulation of Eucalyptus. *Science and Technology Indonesia*, **10**(4); 1074–1086

Sethuram, L. and J. Thomas (2023). Synthesis, Fabrication and Biosafety Profiles of Biobased Microemulsions Reinforced Electrospun Nanofibers for Wound Dressing Applications. *Nano-Structures & Nano-Objects*, **33**; 100940

Sun, Y., Y. Yu, D. Li, W. Kong, and F. Yang (2022). Preparation and Characterization of *Carex meyeriana* Kunth Cellulose Nanofibers by Electrospinning. *Scientific Reports*, **12**(1); 1–14

Xiao, L., J. Liu, M. Z. Hua, and X. Lu (2025). Rapid Determination of Total Phenolic Content and Antioxidant Capacity of Maple Syrup Using Raman Spectroscopy and Deep Learning. *Food Chemistry*, **463**; 141289

Xing, J., M. Zhang, X. Liu, C. Wang, N. Xu, and D. Xing (2023). Multi-Material Electrospinning: From Methods to Biomedical Applications. *Materials Today Bio*, **21**; 100710

Yan, J., S. He, L. Chen, H. Chen, and W. Wang (2023). Characterization, Antioxidant and Antibacterial Activities of Gelatin-Chitosan Edible Coated Films Added with *Cyclocarya paliurus* Flavonoids. *International Journal of Biological Macromolecules*, **253**; 127664

Yang, Y., C. Peng, D. Zeng, Z. Yang, X. Wang, S. Zhang, Y. Bai, L. Kuang, L. Guo, Y. Qin, H. Xiong, J. Wan, C. Yin, T. Ai, Q. Rui, H. Liu, S. Peng, and J. Liu (2024). Electrospinning Is a Potential Way for Preparing Edible Plant Protein-Based Nanofibers with Porous Surface Using Safflower Seed Meal. *Food Hydrocolloids*, **146**; 109201

Zhao, W., S. Cao, H. Cai, Y. Wu, Q. Pan, H. Lin, J. Fang, Y. He, H. Deng, and Z. Liu (2022). Chitosan/Silk Fibroin Biomimic Scaffolds Reinforced by Cellulose Acetate Nanofibers for Smooth Muscle Tissue Engineering. *Carbohydrate Polymers*, **298**; 120056

Zou, X., S. Jiang, Z. Luo, T. Wang, F. Chen, J. Ju, S. Lin, W. Jin, J. Yin, and C. Yang (2025). A Safe and High-Precision Detection Method for Hydrogen Leakage Analysis of Underground Gas Storage Based on Stimulated Raman Spectroscopy of H_2. *Fuel*, **400**; 135743

